

Article

Flexible, Heat-Resistant, and Flame-Retardant Glass Fiber Nonwoven/Glass Platelet Composite Separator for Lithium-Ion Batteries

Ulrich Schadeck ^{1,*}, Kanat Kyrgyzbaev ¹, Heiko Zettl ², Thorsten Gerdes ¹ and Ralf Moos ³

¹ Department of Materials Processing, University of Bayreuth, 95440 Bayreuth, Germany; kanat.kyrgyzbaev@uni-bayreuth.de (K.K.); thorsten.gerdes@uni-bayreuth.de (T.G.)

² Vitrulan Textile Glass GmbH, 95509 Marktschorgast, Germany; h.zettl@vitrulan.com

³ Department of Functional Materials, Zentrum für Energietechnik (ZET), University of Bayreuth, 95440 Bayreuth, Germany; funktionsmaterialien@uni-bayreuth.de

* Correspondence: uli.schadeck@uni-bayreuth.de; Tel.: +49-921-557-216

Received: 26 March 2018; Accepted: 13 April 2018; Published: 20 April 2018



Abstract: A new type of high-temperature stable and self-supporting composite separator for lithium-ion batteries was developed consisting of custom-made ultrathin micrometer-sized glass platelets embedded in a glass fiber nonwoven together with a water-based sodium alginate binder. The physical and electrochemical properties were investigated and compared to commercial polymer-based separators. Full-cell configuration cycling tests at different current rates were performed using graphite and lithium iron phosphate as electrode materials. The glass separator was high-temperature tested and showed a stability up to at least 600 °C without significant shrinking. Furthermore, it showed an exceptional wettability for non-aqueous electrolytes. The electrochemical performance was excellent compared to commercially available polymer-based separators. The results clearly show that glass platelets integrated into a glass fiber nonwoven performs remarkably well as a separator material in lithium-ion batteries and show high-temperature stability.

Keywords: glass platelets; composite separator; high-temperature stability; full-cell configuration cycling tests; lithium-ion battery

1. Introduction

Lithium-ion batteries (LIBs) are widely used for consumer electronics and are promising power sources for electric vehicles (EVs) or hybrid electric vehicles (HEVs) due to their high energy density and efficient cycling stability compared to other battery types [1–5].

The separator is crucial for the safety of a LIB since it physically separates the battery electrodes and prevents internal short circuits. As the cell temperature can rise to critical temperatures, whether in the case of charging at high current rates or in abnormal conditions such as unfortunate overcharge or cell damage, the separator must remain mechanically and chemically stable in order to reduce the risk of serious damage [6,7]. Recent cases of catastrophic battery failures in smartphones were attributed, among other things, to the failure of the separator, which consists of an ultrathin (approx. 4.5 to 5 µm), low-temperature stable polymer membrane with a 1 to 2 µm ceramic coating on one side [8]. Besides its desirable stability at high temperatures, a separator should be well wettable with non-aqueous electrolytes and needs a porous structure for a preferably unimpeded flow of ions to enable fast charging/discharging of a LIB [9,10].

Microporous polyolefin-based membranes consisting of polyethylene (PE) or polypropylene (PP) used to be the standard choice as separators for LIBs. They are easy to process and show decent mechanical and chemical stabilities at an acceptable cost [4]. On the other hand, the poor stability

at high temperatures and the concomitant effect of shrinking, as well as high specific resistances, are prohibitive for their use in high-power applications such as for EVs or for HEV [11,12].

To improve polyolefin-based separators toward high-temperature stability, they are either coated with inorganic micrometer-sized particles or with more temperature-stable polymers [13]. These composite separators show improved stability to high temperatures, wettability with non-aqueous electrolytes, and electrochemical performance in a LIB [14–16]. Porous membranes made with more thermally stable polymers, such as polyacrylonitrile (PAN), polyimide (PI), or melamine-resin, mostly in the shape of nanofibers, show reduced shrinking at temperatures up to 300 °C and good battery performance [17–30]. Nevertheless, the thermal stability is still limited to the melting points of the used polymers or even lower if a polymer tends to shrink. Therefore, high-temperature-stable, non-shrinking materials such as glass or ceramics could be used for separators [12].

As ceramic particles are mostly applied in combination with different polymers, glass is hardly used as a material for separators for organic solvent-based LIBs. However, some promising results have been reported with preparations of glass- or ceramic-based membranes with either glass or ceramic particles or glass fibers with no polymers, with the exception of the binder, respectively [31–33].

Up to now, glass in the shape of micrometer-sized platelets has not been an object of research for separators for LIBs. Today, glass platelets are used in polymer matrices to improve either the mechanical properties and/or the chemical stability [34]. In addition, metal oxide-coated glass platelets are used as pigment additives for paintings and cosmetics [35]. Glass fibers serve, e.g., as the basis for reinforcements for automotive applications, for thermal insulation purposes, and for wallpapers [36–38]. Additionally, applications as separators for lead-acid batteries have been reported [39] and studies regarding their potential as candidates for separators for Li-S batteries have shown promising results [40].

In this work, a high-temperature-stable, self-supporting, and flexible composite separator for liquid electrolyte lithium-ion batteries that consist of a glass fiber nonwoven with integrated custom-made micrometer-sized glass platelets is presented. It is a continuation of our previous study [41], in which the electrochemical properties of single porous and non-porous glass platelets as separators have been studied. In the present study, important properties for self-supporting battery separators such as the tensile strength, the wettability, the electrolyte uptake, and the thermal stability, as well as the electrochemical behavior in graphite/lithium iron phosphate full-cells are studied, mostly compared to commercially available polymer-based separators.

2. Results

2.1. Physical Properties

2.1.1. Morphology

The scanning electron micrographs of the starting materials for the glass composite separator are shown in Figure 1.

The glass platelets showed a flat surface and in the case of ground glass platelets, an average particle size below 32 μm ($d_{50} = 23.1 \mu\text{m}$) and a thickness that was determined to an average value below 5 μm . The resulting aspect ratio was 1:6 to 1:10. In this study, the glass platelets were ground in a jet mill. The glass fiber nonwoven showed straight glass fibers with an average length of 12 mm and diameter of 10 μm . The scanning electron microscopy (SEM) images show residues of the binder, a modified polycarboxylic acid (detailed view in Figure 1b). According to the nonwoven manufacturer's data sheet, the thickness of the glass fiber nonwoven was 300 μm . The measured thickness of 188 μm was less than the stated value due to interlacing of the fibers during measuring.

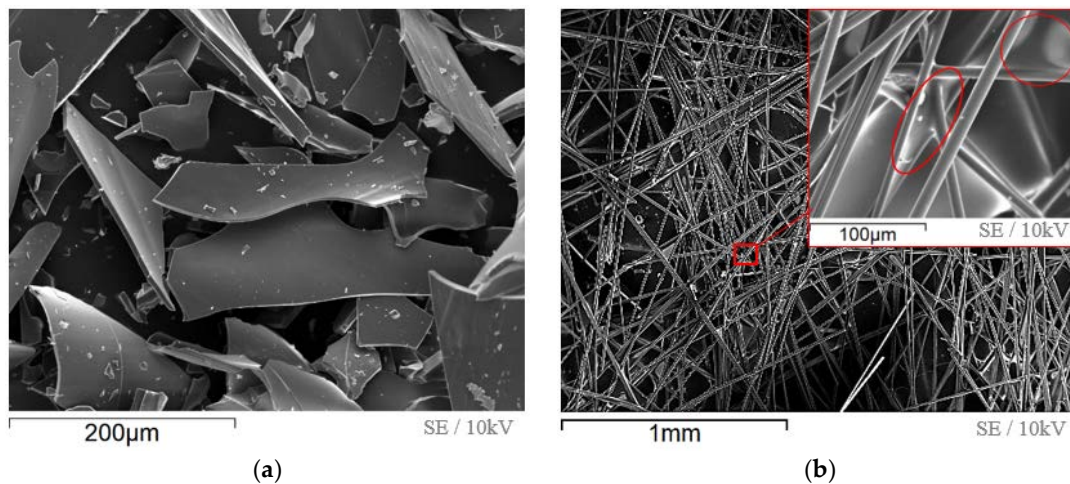


Figure 1. Scanning electron microscopy (SEM) images of the starting materials of a glass composite separator, (a) non-ground glass platelets, (b) glass fiber nonwoven (Johns Manville, Denver, CO, USA) with binder residues between single glass fibers from the nonwoven manufacturing process (detailed view).

The composite separator was manufactured by a tape casting process (see Section 3.2). After the process, the glass platelets were well aligned in the glass composite separator in a horizontal direction, embedded in the glass fiber nonwoven as can be seen from the top view (Figure 2a) and the bottom view (Figure 2b). Figure 3a,b shows the appearance of the separator and a demonstration of its flexibility. A satisfying integration process of the glass platelets into the glass fiber nonwoven with just one tape-casting step is influenced by three major criteria: the viscosity of the platelet-binder slurry; the platelet dimensions, e.g., the average edge length; and the specific size of the fiber interspaces in the glass fiber nonwoven. When the average platelet dimensions are bigger than the average sizes of the interspaces between the glass fibers, an integration of the platelets from top to bottom is hindered. Binder residues, as marked in Figure 2b, are another hindering factor in the integration process. Therefore, smaller glass platelets can penetrate the glass fiber network more easily. An illustration of the platelet integration process is shown in Figure 4. The integration process can be divided into three parts. First, the glass platelets do not have any specific alignment in the platelet-binder slurry (I). Then, through the influence of the moving and angled doctor-blade, the platelets are mostly aligned in a horizontal direction (II) and then pushed inside the glass fiber nonwoven (III).

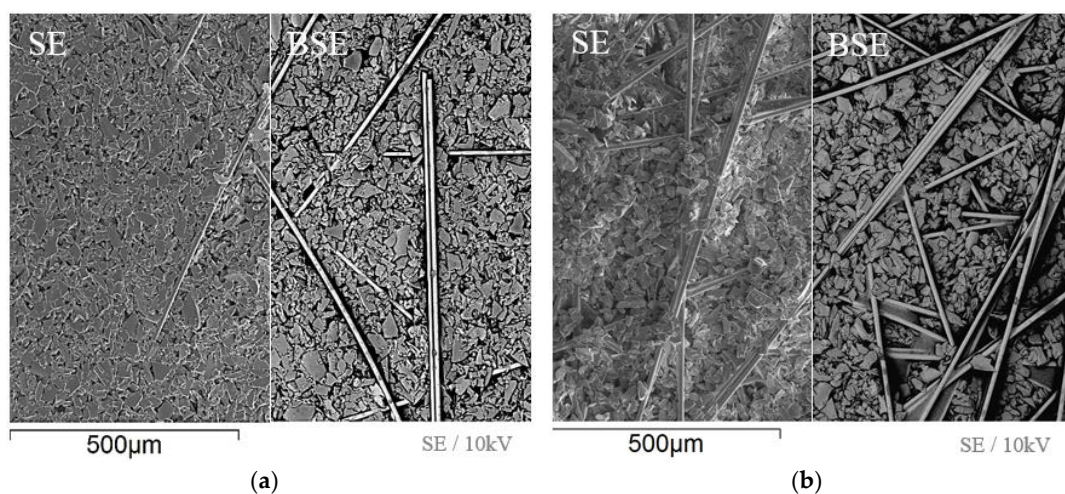


Figure 2. Scanning electron microscopy (SEM) images of a glass fiber nonwoven/glass platelet composite separator, (a) top view; (b) bottom view.

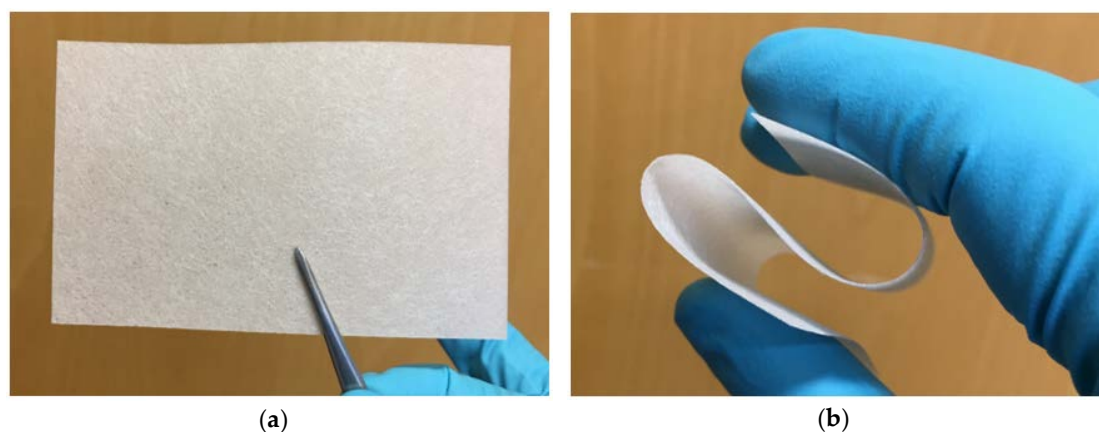


Figure 3. Pictures of a glass fiber nonwoven/glass platelet composite separator, (a) top view; (b) demonstration of the separators flexibility.

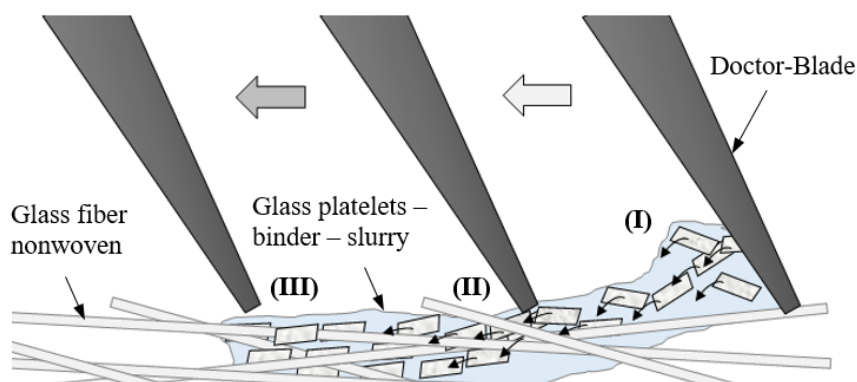


Figure 4. Illustration of the integration process of micrometer-sized glass platelets in a glass fiber nonwoven by tape casting.

Moreover, the sedimentation of the platelets inside the slurry during tape casting plays an important role. For this reason, the viscosity of the slurry is crucial for good platelet integration. If the slurry is too viscous, sedimentation of the platelets inside the binder matrix is hindered, whereas in a low-viscous slurry, the nonwoven is filled with a smaller amount of platelets. Certain values for the viscosity cannot be provided due to the dependency on the various process parameters mentioned above that must always be adapted to the specific properties of the glass fiber nonwoven used. In the case of glass platelets with average dimensions smaller than $32\ \mu\text{m}$ in combination with a premixed sodium alginate binder (ratio water:binder 9:1), with the used glass fiber nonwoven and a feed rate of the doctor-blade of $2.5\ \text{mm/s}$, the viscosity should be between $10^2\ \text{Pa s}$ and $10^4\ \text{Pa s}$.

The average thickness of the final composite was $207\ \mu\text{m}$, i.e., no significant thickness increase occurred compared to the bare nonwoven. The porosity of the composite was 30–35% with an average pore size of $1\text{--}3\ \mu\text{m}$.

Since the final thickness of the presented composite separator was around $200\ \mu\text{m}$, it was significantly thicker than commercial polymer-based separators that are usually $20\text{--}30\ \mu\text{m}$ thick [42]. The average area weight of the presented glass composite separator was $80\text{ to }100\ \text{g/m}^2$ (polymer-based separators $20\text{--}40\ \text{g/m}^2$ [42]). Taking the thickness into account, the base-weight of the presented glass separator was even lower than the polymer separators. The high thickness affects the overall volumetric and/or gravimetric energy density of a battery cell and makes further optimization toward a lower area weight indispensable.

2.1.2. Thermal Stability

The thermal stability of the described glass composite separator was tested with a so-called hot oven test (Figure 5a) and thermogravimetric analysis (Figure 5b), as well as with a so-called hot-punch test (Figure 5c). For the demonstration of its low flammability, the separator was tortured with a gas burner. The results of the hot oven and the hot punch test were compared to commercially available polymer-based separators, a polymer trilayer (PTS), and a ceramic-coated polymer separator (CCPS). Thermogravimetric measurements of commercially available polymer-based separators compared to bare glass platelets were shown already in the previous study [41].

The shrinkage of various separators was observed in a so-called hot oven test at temperatures from 100 to 600 °C in steps of 100 °C and extra steps at 166 °C and 250 °C, indicating the melting points of the used PP and PET of the polymer-based separators PTS and CCPS. The results are shown in Figure 5a. To calculate the particular shrinkage, the average change of the samples' edge lengths was used according to Equation (2).

The hot oven test (see Figure 5a) shows a comparatively low stability to high temperatures of the PTS. The PE inner layer started to melt at 135 °C, indicated by a color change from white to clear. The shrinkage began at temperatures above 166 °C, which is approximately the melting point of the PP outer layers. The PTS was completely melted at 250 °C. The CCPS was more stable with respect to high temperatures due to its ceramic coating and the used PET mesh core, which is more thermally stable than PE or PP. Nevertheless, the inner polymer mesh of the membrane started to melt above 250 °C, which is reflected by the observed shrinkage. When tortured with minimal pressure (flat load; 50 g cm⁻²), the membrane shattered into parts whereas the glass composite separator was mechanically stable with just a few detached glass platelets (see Figure 5a). Additionally, the glass composite separator showed minimal shrinkage even at temperatures up to 600 °C.

The resulting thermogravimetric curve is divided into three major sections (Figure 5b). At first, moisture (I) and then residues of the polycarboxylic-based binder (II) in the glass fiber nonwoven left the sample. The third part indicates the weight loss originating from the alginate-based binder. In summary, a weight loss of approximately 8% was observed at temperatures of 585 °C. In comparison, commercial polymer-based separators show a weight loss of 25% (ceramic-coated polymer separator) and >95% (polymer trilayer separator) at 585 °C [41].

Since the hot copper pin was not touching the separators during the hot punch test, the heat was transmitted via heat radiation. As can be seen in Figure 5c, a hole was melted in the PTS after a few seconds. The CCPS and the glass separator showed no significant change and it can be assumed that the physical separation of the two electrodes was still be guaranteed even though the membranes were touched with the hot copper pin. Since no polymer was used, not even as a binder, and the amount of alginate used was not sufficient to be flammable, the glass composite separator can be described as being flame-retardant (Figure 5d).

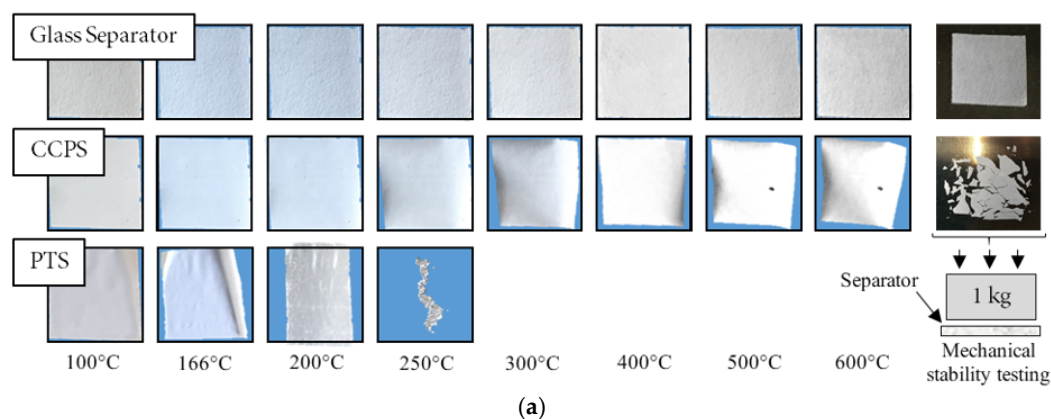


Figure 5. Cont.

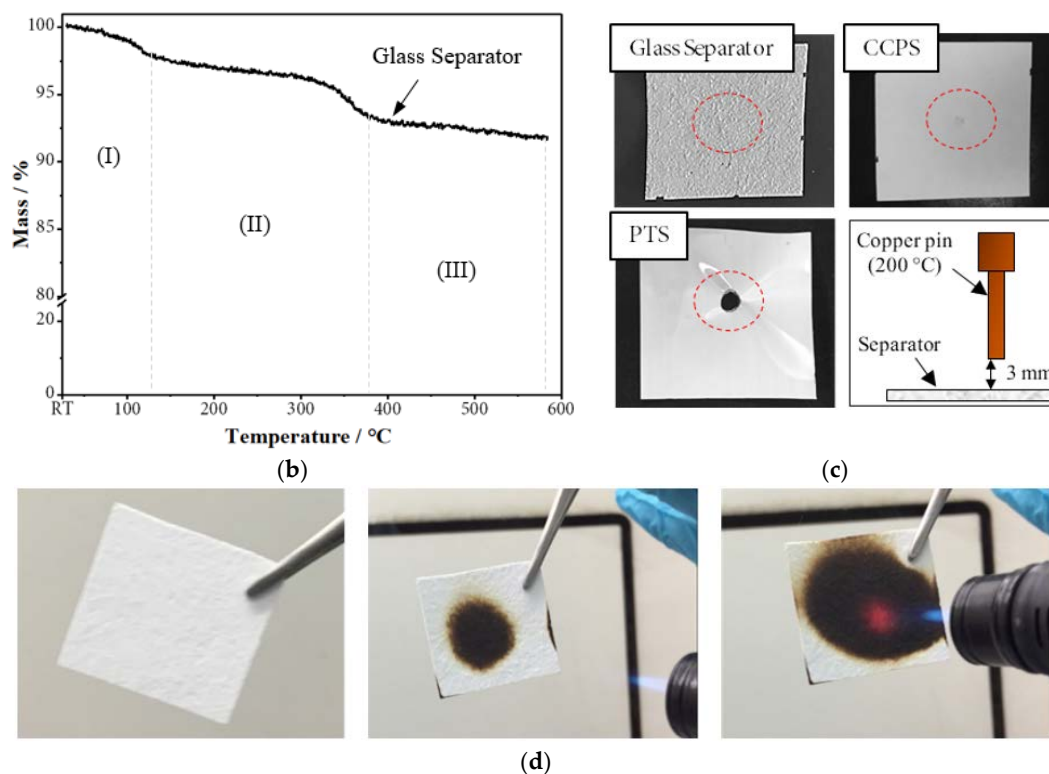


Figure 5. Thermal stability of a glass fiber nonwoven/glass platelet composite separator, (a) temperature-dependent shrinkage (hot-oven test) compared to polymer-based separators; (b) thermogravimetric analysis; (c) behavior at exposures to 200 °C by heat radiation (hot-punch test); (d) demonstration of the flame retardation of the glass composite separator.

2.1.3. Wettability

The wettability of battery separators is crucial for fast cell manufacturing [42]. In order to evaluate the wettability of the comparative separators, the contact angles, as well as the electrolyte uptake, were measured. As no measurement was possible using a standard battery electrolyte, the electrolyte solvent DMC (10 μ L) served as the test liquid.

Since wetting of a separator with electrolyte is a dynamic process, it is necessary to observe how the wetting process evolves over time. Figure 6a–c are images of static contact angles of the glass composite separator and the compared polymer-based separators CCPS and PTS, taken at identical times after DMC contact (0 to 60 ms/20 ms steps). CCPS showed quite good wettability with DMC. A contact angle of 11–21° was observed. Owing to the non-polar surface charge of the used polymers, wetting of PTS took more time. Moreover, the average pore size of PTS was bigger than in CCPS. Consequently, a comparably high contact angle of >20° was measured, even after the same time that was needed for the CCPS to soak up all the DMC. The glass composite separator also showed very good wettability, as indicated by a rapidly decreasing contact angle that was always smaller than 20°. The defined amount of DMC was completely soaked in <50 ms. In comparison, 1–1.5 s for the CCPS and more than 60 s for the PTS were needed to soak the same amount of DMC.

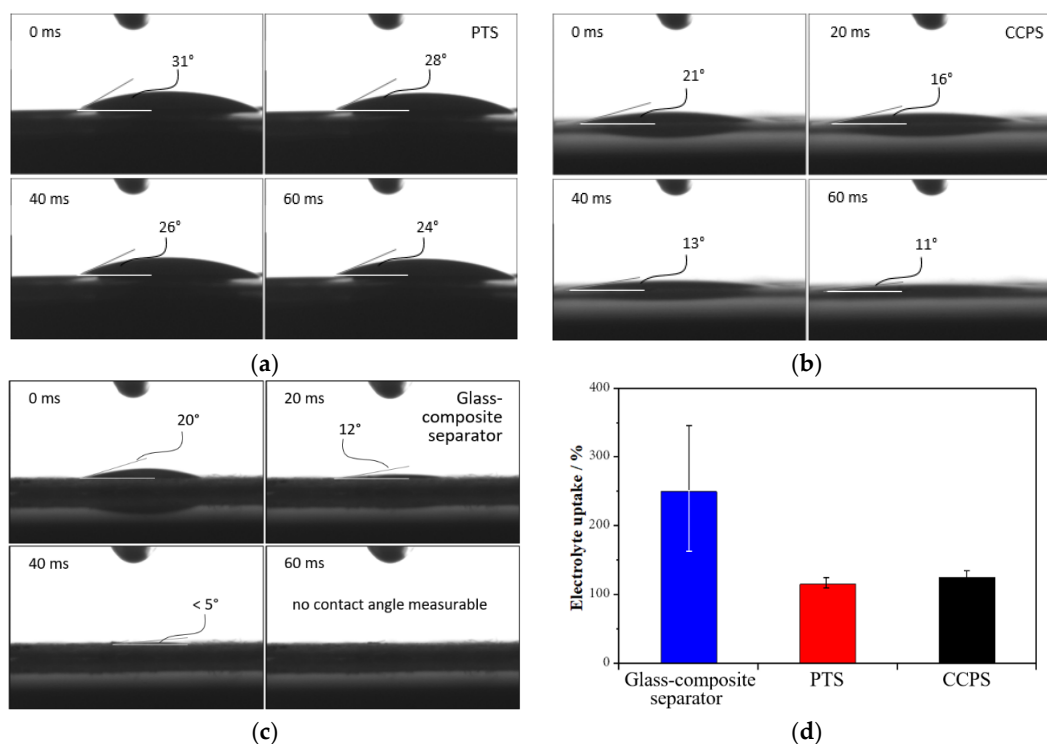


Figure 6. Photographs of the contact angle measured with 10 μL DMC (a) polymer trilayer separator (PTS); (b) ceramic-coated polymer separator (CCPS); (c) glass composite separator; (d) electrolyte uptake of glass composite separator compared to PTS and CCPS.

The electrolyte uptake was measured with samples of the glass composite separator and the polymer separators. Depending on the average platelet dimensions, the binder content, and the filling degree of platelets in the glass fiber nonwoven, an electrolyte uptake of the glass composite separator between 155 and 345 wt % was measured. For the CCPS and the PTS, an electrolyte uptake of 115 and 125% by weight was determined, respectively (see Figure 6d). We determined that the best electrolyte uptake goes hand-in-hand with a systematic reduction in the binder content to 1 to 2% by weight and an adjustment in the average pore size to 1–3 μm , which is significantly larger than commercial separators that usually have pores with a size around 0.04 to 0.09 μm (PTS) or 0.3 μm (CCPS) [42]. Another benefit for an improved electrolyte uptake was the hydrophilic glass surface.

2.1.4. Mechanical Stability

Samples of the here-investigated glass composite separator, as well as the polymer-based separators, were fixed and stretched in a tensile testing machine. Figure 7a depicts the results.

On the one hand, the glass composite separator showed no significant difference in the machine direction (MD) and transverse direction (TD) and could be loaded with the highest tensile force due to the comparatively high thickness. However, the glass separator showed the poorest strain ($\sim 3\%$) at an acceptable tension, which was comparable to the same of a CCPS measured in MD. We attributed the low tensile strength to the low ductility of the glass fibers themselves. With the integration of the glass platelets, the composites became even stiffer, even though the tension increased by a factor of two compared to an unfilled nonwoven. In comparison, polymer-based separators showed a significantly higher tensile strength, especially PTS, at least in MD.

In addition to the tensile strength, the puncture strength was tested (Figure 7b). Similar to the results of the tensile strength test, the glass composite separator could be loaded with the highest force of a penetrating plane metal tip, which again was attributed to the higher thickness. Furthermore, the PTS separator was first stretched to a puncture force of 3.5 N before its inner polymer bondings

between the contrary polymer webs were torn (1). At this point, the separator was faulty and could no longer guarantee a physical separation of the two electrodes in the battery cell. The remaining polymer webs were further stretched until snapping (2). The CCPS separator showed the lowest puncture strength due to the comparable coarse polymer mesh, which allowed easy penetration of the metal sphere.

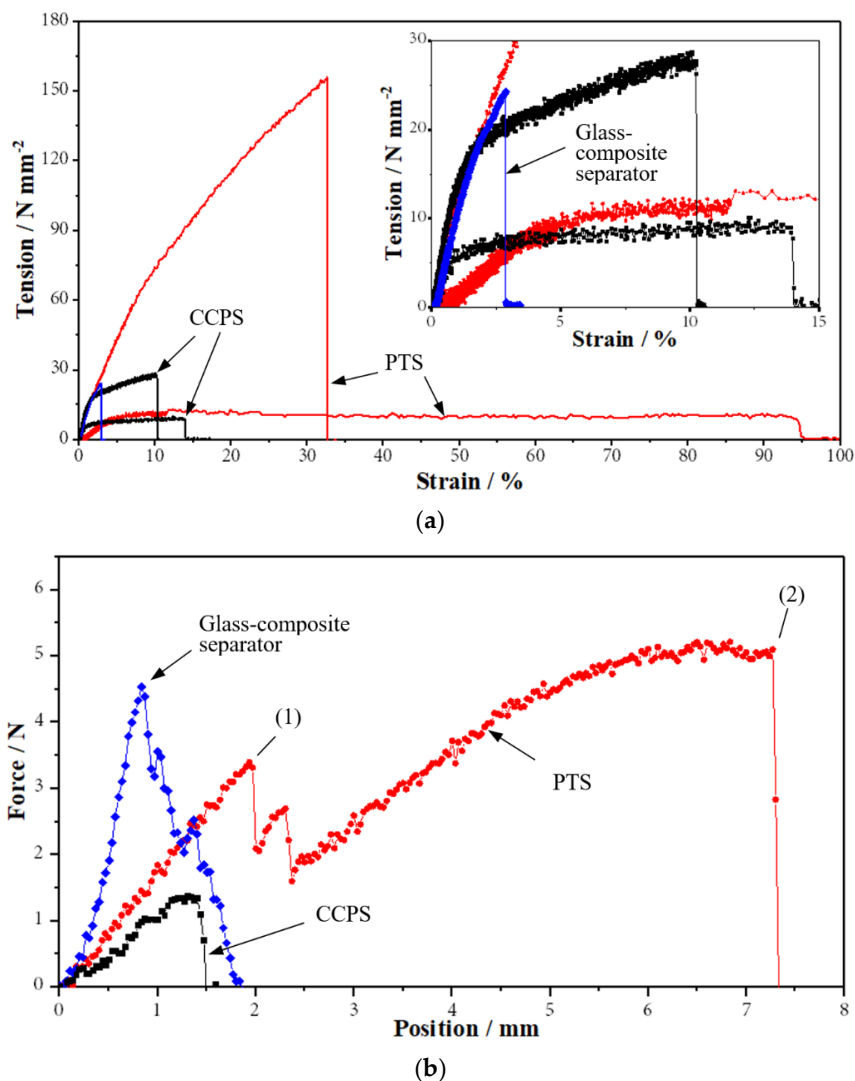


Figure 7. Mechanical stability of a glass composite separator, CCPS, and PTS, (a) tensile strength in the machine direction (MD) and transverse direction (TD); (b) puncture strength.

2.2. Electrochemical Properties

The glass composite separator, as well as the PTS and the CCPS, was charged/discharged in a full-cell configuration setup. Therefore, graphite served as the anode and LFP as the cathode. After cell preparation, five cycles with different current rates (C-rate) were performed for a defined formation of the cell. After cell formation, a constant current rate of 1 C at a DoD (depth of discharge) of 100% impinged 95 consecutive cycles. Figure 8a shows the capacity retention of the prepared glass-based separator compared to PTS and CCPS. In addition, the rate capability at current rates of 1 C, 2 C, 5 C, and 10 C was measured (Figure 8b) after the capacity retention test with a constant C-rate as shown in Figure 8a. The test cells were all equipped with the same amount of active material leading to a starting cell capacity of 2.38 mAh (± 0.01 mAh).

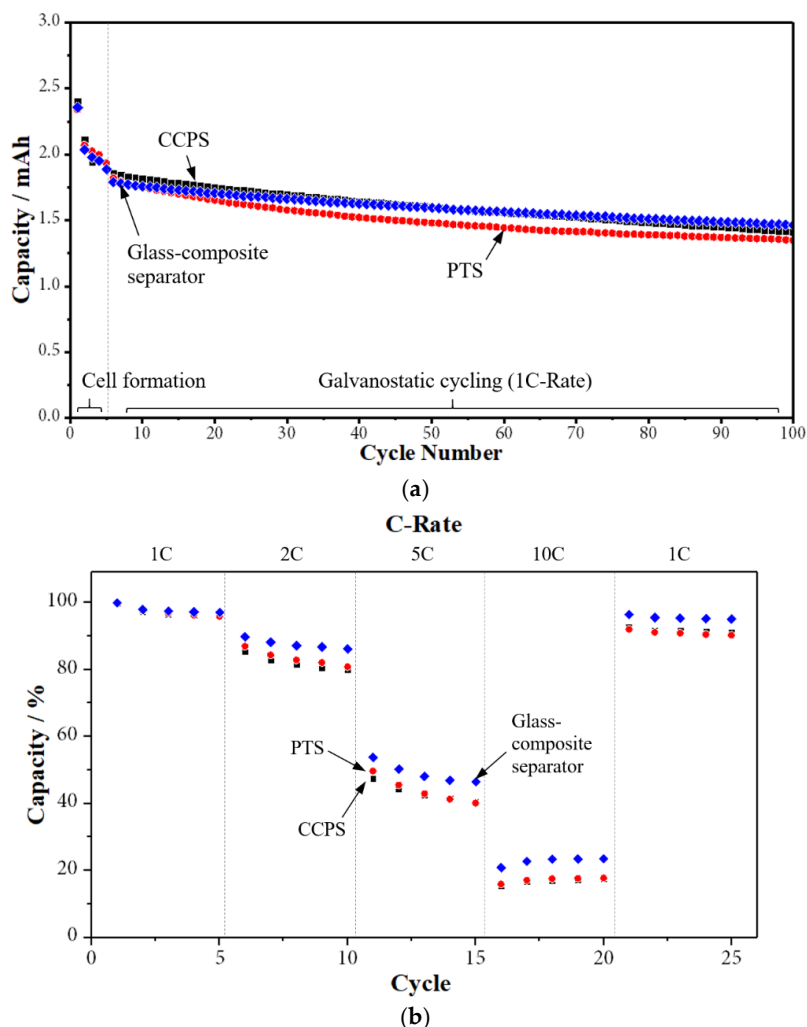


Figure 8. Battery performance of a glass composite separator, a PTS, and a CCPS in a graphite/LFP full-cell configuration (a) cell formation progressing cycling at 1 C-rate; (b) rate capability at a 1 C, 2 C, 5 C, and 10 C-rate after previous cycling at a 1 C-rate for 95 cycles and cell formation.

The initial capacity loss of a test cell with a glass composite separator was measured to 13.6%, which is slightly higher compared to cells with polymer-based separators. A test cell with CCPS showed an initial capacity loss of 12.5% and with PTS 11.6%. It was assumed that there were undesired side reactions between the glass and the battery electrolyte. The tendency of the glass to bind humidity on the glass surface itself, even though the samples were conditioned before cell assembling, could have caused the in situ formation of hydrofluoric acid, which would have caused electrolyte decomposition and/or aluminum current collector passivation [43]. Since the difference in the initial capacity loss was just 1% to 2% and if the further course of the capacity loss per cycle was compared, it was considered negligible.

During galvanostatic cycling for 95 continuous cycles at a constant current rate (1 C rate), a capacity loss of 17.8% was measured for the test cell with a glass separator. The average Coulomb efficiency (CE) was calculated to >99.7% at any time (calculation without cell formation). In comparison, a test cell with CCPS showed a capacity loss of 28.7% after galvanostatic cycling (average CE of 99.5). The PTS showed a similar battery performance as CCPS (average CE of 99.5%) but a slightly different progression of the capacity fade, which was comparably higher in the first 50 cycles and stabilized after that.

Subsequently, in addition to the test of the capacity retention at a constant C-rate of 1 C, we compared the rate capability of the cycled test cells. Therefore, a current rate up to a 10 C-rate was

applied. The rate capability of a test cell with the described glass composite separator was compared to CCPS and PTS (Figure 8b). Concerning the test cell with the glass separator, an average capacity of 23% was charged/discharged at a 10 C-rate, whereas a test cell with a CCPS or a PTS separator was charged only up to 16–17% of capacity. Similar effects were shown at current rates of 2 C and 5 C, respectively. After cycling at a 10 C rate, five cycles at a 1 C rate were performed. The test cell with a the glass composite separator showed a total capacity loss of 4.5% as part of this test, while the capacity of the comparative test cells with a CCPS or a PTS was degraded to 8.5 and 9%, respectively.

In summary, the capacity retention, as well as the rate capability of test cells with the glass composite separator, was slightly improved compared to cells with polymer-based separators. Besides the physical properties such as the bigger pore sizes and the easy wetting or bigger solvent uptake of the glass separator, we attributed this improvement to the interaction between the glass and battery electrolytes. It is known that specific electrolyte additives can enhance the performance of lithium-ion batteries [44]. It is assumed that ions from the glass, which are dissolved in the electrolyte in unexpected side reactions, are responsible for the improved electrochemical behavior.

3. Materials and Methods

3.1. Materials

The glass (Telux Glasproducts & Components GmbH, Weißwasser, Germany) for preparing the glass platelets was a sodium borosilicate glass with traces of zirconium oxide, aluminum oxide, titanium oxide, potassium oxide, and barium oxide. Further details are described in [41]. A glass fiber nonwoven was purchased (Johns Manville Corp., Denver, CO, USA). As a binder, water-based sodium alginate (Sigma Aldrich, St. Louis, MO, USA) was used. A graphite-coated copper foil served as the anode, the cathode consisted of an aluminum foil with a lithium iron phosphate coating. Both electrodes were commercially obtained (Customcells Itzehoe GmbH, Itzehoe, Germany) in the balanced configuration (2.2 mAh/cm² for the graphite, 2.0 mAh/cm² for the LFP). A commercial LP30 served as the electrolyte (1:1 EC:DMC, 1 mol dm⁻³ LiPF₆; Merck & Co., Kenilworth, NJ, USA). A ceramic-coated PET-nonwoven separator (Separion[®] S240P30; Evonik Industries AG, Essen, Germany) denoted as CCPS (thickness 28.5 µm) and a polymer trilayer (Celgard[®] 2325, Celgard LLC, Charlotte, NC, USA) denoted as PTS (thickness 25 µm) were used to compare our data with commercially available separators.

3.2. Preparation of a Glass Platelet—Glass Fiber Nonwoven Composite Separator

To manufacture the micrometer-sized glass platelets, a rotary atomization process was used. The glass was melted at 1350 °C in a glass melting tank. After melting, the glass melt was then fed into a rotating and preheated atomizer (cup-shaped). Due to the rotation of the atomizer, the glass melt was pushed outwards over the edge of the atomizer and formed lamellae. These lamellae were further stretched and simultaneously quenched until the glass broke, resulting in micrometer-sized glass platelets. Further details of the process are described by Kyrgyzbaev et al. [45] and Schadeck et al. [41].

The glass platelets (average thickness <5 µm) were ground and sorted by particle size. Platelets with an average particle size <32 µm were used to prepare the glass composite separator. The binder was obtained by stirring a defined amount of sodium alginate with deionized water (ratio 1:9) for 48 h at room temperature. After that, the binder was mixed with the glass platelets in a centrifugal mixer (Thinky Mixer ARE 250 CE, Laguna Hill, CA, USA) for 5 min/1200 rpm to obtain a homogeneous slurry. Then, a doctor blade was used to cast the glass platelet-binder slurry inside the glass fiber nonwoven at a feed speed of 2.5 mm s⁻¹. Therefore, the height of the doctor blade was adjusted to 90% of the premeasured height of the glass fiber nonwoven. Finally, the composites were conditioned in a vacuum furnace at 80 °C for at least 4 h. To prepare samples for electrochemical characterizations, discs (Ø 12 mm) were punched.

3.3. Characterization

The samples of the glass composite separators, as well as the previously punched electrode materials, were conditioned in a tube furnace in a constant flow of Argon ($10 \text{ dm}^3 \text{ h}^{-1}$) at $110 \text{ }^\circ\text{C}$ for 12 h in order to remove any moisture.

Thermogravimetric analysis (TGA; Netzsch, Selb, Germany) was conducted up to $585 \text{ }^\circ\text{C}$ (heating rate $10 \text{ }^\circ\text{C min}^{-1}$; air flow $3 \text{ dm}^3 \text{ h}^{-1}$). The thermal stability of the various separators was determined by measuring the dimensional change of samples (30 mm square) after being exposed to various temperatures up to $600 \text{ }^\circ\text{C}$ for 30 min each. The shrinkage S_{rel} was calculated by Equation (1):

$$S_{rel} (\%) = \frac{A_1 - A_0}{A_0} \times 100 \quad (1)$$

wherein A_0 and A_1 denote the sample surface area before/after the heat treatment. Additionally, and according to [11], a so-called hot punch test was performed where the separator samples were put 3 mm under a preheated metal tip ($200 \text{ }^\circ\text{C}$, diameter 2 mm) for 1 min.

To obtain data of the wettability of the separators, the contact angles were determined. Here, a defined amount of organic solvent ($10 \text{ } \mu\text{L}$ DMC) was dropped on the samples and the contact angle was measured using a static digital photograph taken by the identical time after electrolyte contact (20 ms). The electrolyte uptake u_{rel} was calculated by Equation (2). Therefore, the weight of the samples before (m_0) and after (m) wetting (2 h soaking) was measured.

$$u_{rel} (\%) = \frac{m_0 - m}{m_0} \times 100 \quad (2)$$

The morphologies of the glass platelets, the glass fiber nonwoven, as well as the composite membranes, were investigated using a scanning electron microscope (SEM; JSM-840A, JEOL Ltd., Tokyo, Japan) at an acceleration voltage of 10 kV . The porosity and the average pore diameters of the glass composite separator samples were obtained by gas adsorption (Micromeritics, ASAP 2010, Norcross, GA, USA) and Hg-porosimetry (Micromeritics Auto Pore 9410, Pore-Core, Norcross, GA, USA).

Furthermore, the mechanical stability of the glass composite membrane in comparison to the commercial polymer-based separators was tested. The tensile strength was measured in both the machine direction (MD) and in the transverse direction (TD) where a clamped piece of the separator ($20 \times 80 \text{ mm}$) was stretched (Series 5569, Instron, Norwood, MA, USA) with a feed speed of 1 mm min^{-1} . Additionally, the puncture strength was observed by penetrating the membranes with a rounded steel tip ($\text{Ø} 2 \text{ mm}$). Therefore, discs ($\text{Ø} 14 \text{ mm}$) of the various separators were fixed between two steel flat washers in an open Swagelok $1/2''$ tube fitting.

To investigate the electrochemical parameters, the samples of the glass composite and the commercial polyolefin-based separators were mounted in a Swagelok[®] $1/2''$ tube fitting. Commercial graphite served as the anode and LFP as the cathode (full-cell configuration). The graphite/separator/LFP-sandwich was fixed between two custom-made stainless steel electrodes. The cells were prepared under inert gas conditions in a glovebox.

The capacity retention, as well as the rate capability of the test cells with various separators, was tested in a battery test system (CTS-LAB, BaSyTec GmbH, Asselfingen, Germany). At first, the test cells were formatted (5 cycles; $2 \times 0.1 \text{ C}$, $2 \times 0.5 \text{ C}$, $1 \times 1 \text{ C}$) according to the electrode materials' manufacturer's data sheet. The cell potential served as the termination criterion ($3.8 \text{ V}/2.5 \text{ V}$). For all cycles, a DoD (depth of discharge) of 100% was used. After cell formation, the capacity retention was observed for 95 cycles at a 1 C -rate. The rate capability measurement was conducted after the capacity retention test, wherein different current rates (1 C , 2 C , 5 C , and 10 C) were applied for five cycles each. For that, the same potential range and a DoD of 100% were used as well.

4. Conclusions

A novel type of glass-based separator was prepared using a glass fiber nonwoven with integrated custom-made micrometer-sized glass platelets as a high-temperature stable alternative to polymer-based separators. The physical properties, as well as the battery performance in a graphite/LFP full-cell setup, were tested. Correspondingly, the results were compared to polymer-based separators. The presented glass composite separator is flexible, flame-retardant, and stable up to 600 °C, shows almost no shrinkage (~2%), and is still mechanically stable. Furthermore, fast wetting of non-aqueous electrolytes was observed. The glass composite separator was soaked with organic solvent 20 and 1200 times faster than typical ceramic-coated polymer separators and polymer trilayer separators, respectively. On the other hand, the thickness of the glass composite membrane, as well as the tensile strength, needs to be further improved, even though the results of the puncture strength tests are quite promising. The electrochemical properties of a graphite/LFP full-cell configuration setup were excellent. The Coulomb efficiency was still above 99.7% at a 1 C-rate during galvanostatic cycling and the overall capacity retention was equal and even slightly higher than the typical polymer separators. During rate capability tests, a capacity of 23% was charged/discharged at a 10 C rate, whereas cells with typical polymer-based separators were charged only to 17% of capacity.

It was shown that a glass-based separator made from glass fiber nonwovens with integrated glass platelets is a suitable, high-temperature-stable separator with good battery performance and an excellent wettability for fast cell manufacturing.

Acknowledgments: The financial support by the BayNW project ACoS (PTJ-1308-0002) and the further financial support as part of a graduate program of the TechnologieAllianzOberfranken (TAO) is gratefully acknowledged. This publication was funded by the German Research Foundation (DFG) and the University of Bayreuth in the funding program Open Access Publishing. This work is dedicated to Monika Willert-Porada who passed away in 2016. We kindly would like to thank her for her contribution to the project and for her support.

Author Contributions: Ulrich Schadeck wrote the paper and performed all experiments; Kanat Kyrgyzbaev helped in preparing the glass platelets; Heiko Zettl provided the glass fiber nonwoven, shared his know-how about binders, and successfully tested the preparation of glass composite separators in industrial roll-to-roll processes; Thorsten Gerdes initiated the above-mentioned project; Ralf Moos, Thorsten Gerdes, Heiko Zettl, and Kanat Kyrgyzbaev provided guidance, discussed the collected data, helped in manuscript preparation, and decided on the next steps.

Conflicts of Interest: The authors declare no conflicts of interest.

References

1. Lu, L.; Han, X.; Li, J.; Hua, J.; Ouyang, M. A review on the key issues for lithium-ion battery management in electric vehicles. *J. Power Sources* **2013**, *226*, 272–288. [[CrossRef](#)]
2. Park, J.-K. (Ed.) *Principles and Applications of Lithium Secondary Batteries*; Wiley-VCH: Weinheim, Germany, 2012; ISBN 978-3-52-733151-2. [[CrossRef](#)]
3. Linden, D.; Reddy, T.B. (Eds.) *Linden's Handbook of Batteries*, 4th ed.; McGraw-Hill: New York, NY, USA, 2011; ISBN 978-0-07-162421-3.
4. Cairns, E.J.; Albertus, P. Batteries for electric and hybrid-electric vehicles. *Annu. Rev. Chem. Biomol. Eng.* **2010**, *1*, 299–320. [[CrossRef](#)] [[PubMed](#)]
5. Gerssen-Gondelach, S.J.; Faaij, A.P.C. Performance of batteries for electric vehicles on short and longer term. *J. Power Sources* **2012**, *212*, 111–129. [[CrossRef](#)]
6. Abada, S.; Marlair, G.; Lecocq, A.; Petit, M.; Sauvant-Moynot, V.; Huet, F. Safety focused modeling of lithium-ion batteries, A review. *J. Power Sources* **2016**, *306*, 178–192. [[CrossRef](#)]
7. Nazri, G.-A.; Pistoia, G. (Eds.) *Lithium Batteries: Science and Technology*, 1st ed.; Springer: New York, NY, USA, 2009; ISBN 978-0-38-792675-9.
8. Loveridge, M.; Remy, G.; Kourra, N.; Genieser, R.; Barai, A.; Lain, M.; Guo, Y.; Amor-Segan, M.; Williams, M.; Amietszajew, T.; et al. Looking Deeper into the Galaxy (Note 7). *Batteries* **2018**, *4*, 3. [[CrossRef](#)]
9. Huang, X. Separator technologies for lithium-ion batteries. *J. Solid State Electrochem.* **2011**, *15*, 649–662. [[CrossRef](#)]

10. Yang, M.; Hou, J. Membranes in lithium ion batteries. *Membranes* **2012**, *2*, 367–383. [[CrossRef](#)] [[PubMed](#)]
11. Shi, C.; Zhang, P.; Chen, L.; Yang, P.; Zhao, J. Effect of a thin ceramic-coating layer on thermal and electrochemical properties of polyethylene separator for lithium-ion batteries. *J. Power Sources* **2014**, *270*, 547–553. [[CrossRef](#)]
12. Roth, E.P.; Doughty, D.H.; Pile, D.L. Effects of separator breakdown on abuse response of 18,650 Li-ion cells. *J. Power Sources* **2007**, *174*, 579–583. [[CrossRef](#)]
13. Kim, J.Y.; Lim, D.Y. Surface-Modified Membrane as a Separator for Lithium-Ion Polymer Battery. *Energies* **2010**, *3*, 866–885. [[CrossRef](#)]
14. Huang, F.; Liu, W.; Li, P.; Ning, J.; Wei, Q. Electrochemical Properties of LLTO/Fluoropolymer-Shell Cellulose-Core Fibrous Membrane for Separator of High Performance Lithium-Ion Battery. *Materials* **2016**, *9*, 75. [[CrossRef](#)] [[PubMed](#)]
15. Choi, J.-A.; Kim, S.H.; Kim, D.-W. Enhancement of thermal stability and cycling performance in lithium-ion cells through the use of ceramic-coated separators. *J. Power Sources* **2010**, *195*, 6192–6196. [[CrossRef](#)]
16. Shi, C.; Dai, J.; Li, C.; Shen, X.; Peng, L.; Zhang, P.; Wu, D.; Sun, D.; Zhao, J. A Modified Ceramic-Coating Separator with High-Temperature Stability for Lithium-Ion Battery. *Polymers* **2017**, *9*, 159. [[CrossRef](#)]
17. Zhai, Y.; Xiao, K.; Yu, J.; Ding, B. Fabrication of hierarchical structured SiO₂/polyetherimide-polyurethane nanofibrous separators with high performance for lithium ion batteries. *Electrochim. Acta* **2015**, *154*, 219–226. [[CrossRef](#)]
18. Yeon, D.; Lee, Y.; Ryou, M.-H.; Lee, Y.M. New flame-retardant composite separators based on metal hydroxides for lithium-ion batteries. *Electrochim. Acta* **2015**, *157*, 282–289. [[CrossRef](#)]
19. Yanilmaz, M.; Zhang, X. Polymethylmethacrylate/Polyacrylonitrile Membranes via Centrifugal Spinning as Separator in Li-Ion Batteries. *Polymers* **2015**, *7*, 629–643. [[CrossRef](#)]
20. Yanilmaz, M.; Dirican, M.; Zhang, X. Evaluation of electrospun SiO₂/nylon 6,6 nanofiber membranes as a thermally-stable separator for lithium-ion batteries. *Electrochim. Acta* **2014**, *133*, 501–508. [[CrossRef](#)]
21. Shi, C.; Dai, J.; Huang, S.; Li, C.; Shen, X.; Zhang, P.; Wu, D.; Sun, D.; Zhao, J. A simple method to prepare a polydopamine modified core-shell structure composite separator for application in high-safety lithium-ion batteries. *J. Membr. Sci.* **2016**, *518*, 168–177. [[CrossRef](#)]
22. Lee, J.; Lee, C.-L.; Park, K.; Kim, I.-D. Synthesis of an Al₂O₃-coated polyimide nanofiber mat and its electrochemical characteristics as a separator for lithium ion batteries. *J. Power Sources* **2014**, *248*, 1211–1217. [[CrossRef](#)]
23. Jiang, W.; Liu, Z.; Kong, Q.; Yao, J.; Zhang, C.; Han, P.; Cui, G. A high temperature operating nanofibrous polyimide separator in Li-ion battery. *Solid State Ion.* **2013**, *232*, 44–48. [[CrossRef](#)]
24. Song, J.; Ryou, M.-H.; Son, B.; Lee, J.-N.; Lee, D.J.; Lee, Y.M.; Choi, J.W.; Park, J.-K. Co-polyimide-coated polyethylene separators for enhanced thermal stability of lithium ion batteries. *Electrochim. Acta* **2012**, *85*, 524–530. [[CrossRef](#)]
25. Miao, Y.-E.; Zhu, G.-N.; Hou, H.; Xia, Y.-Y.; Liu, T. Electrospun polyimide nanofiber-based nonwoven separators for lithium-ion batteries. *J. Power Sources* **2013**, *226*, 82–86. [[CrossRef](#)]
26. Smith, S.A.; Williams, B.P.; Joo, Y.L. Effect of polymer and ceramic morphology on the material and electrochemical properties of electrospun PAN/polymer derived ceramic composite nanofiber membranes for lithium ion battery separators. *Annu. Rev. Chem. Biomol. Eng.* **2017**, *526*, 315–322. [[CrossRef](#)]
27. Khan, W.S.; Asmatulu, R.; Rodriguez, V.; Ceylan, M. Enhancing thermal and ionic conductivities of electrospun PAN and PMMA nanofibers by graphene nanoflake additions for battery-separator applications. *Int. J. Energy Res.* **2014**, *38*, 2044–2051. [[CrossRef](#)]
28. Yanilmaz, M.; Lu, Y.; Li, Y.; Zhang, X. SiO₂/polyacrylonitrile membranes via centrifugal spinning as a separator for Li-ion batteries. *J. Power Sources* **2015**, *273*, 1114–1119. [[CrossRef](#)]
29. Lee, J.H.; Manuel, J.; Choi, H.; Park, W.H.; Ahn, J.-H. Partially oxidized polyacrylonitrile nanofibrous membrane as a thermally stable separator for lithium ion batteries. *Polymer* **2015**, *68*, 335–343. [[CrossRef](#)]
30. Wang, Q.; Yu, Y.; Ma, J.; Zhang, N.; Zhang, J.; Liu, Z.; Cui, G. Electrospun melamine resin-based multifunctional nonwoven membrane for lithium ion batteries at the elevated temperatures. *J. Power Sources* **2016**, *327*, 196–203. [[CrossRef](#)]
31. Carvalho, D.V.; Loeffler, N.; Kim, G.-T.; Passerini, S. High Temperature Stable Separator for Lithium Batteries Based on SiO₂ and Hydroxypropyl Guar Gum. *Membranes* **2015**, *5*, 632–645. [[CrossRef](#)] [[PubMed](#)]

32. Luo, X.; Pan, W.; Liu, H.; Gong, J.; Wu, H. Glass fiber fabric mat as the separator for lithium-ion battery with high safety performance. *Ionics* **2015**, *21*, 3135–3139. [[CrossRef](#)]
33. Jung, Y.-C.; Kim, S.-K.; Kim, M.-S.; Lee, J.-H.; Han, M.-S.; Kim, D.-H.; Shin, W.-C.; Ue, M.; Kim, D.-W. Ceramic separators based on Li⁺-conducting inorganic electrolyte for high-performance lithium-ion batteries with enhanced safety. *J. Power Sources* **2015**, *293*, 675–683. [[CrossRef](#)]
34. Brigham, S.J.; Watkinson, C. Understanding and use of glass flake. *Paint Coat. Ind.* **2009**, *25*, 22–24.
35. Anselmann, R.; Ambrosius, K.; Mathias, M. Effect Pigments Based on Coated Glass Flakes. U.S. Patent 7,226, 503, 5 June 2007.
36. Koronis, G.; Silva, A.; Fontul, M. Green composites, a review of adequate materials for automotive applications. *Composites Part B* **2013**, *44*, 120–127. [[CrossRef](#)]
37. Kaynakli, O. A review of the economical and optimum thermal insulation thickness for building applications. *Renew. Sustain. Energy Rev.* **2012**, *16*, 415–425. [[CrossRef](#)]
38. Aleksic, B.; Bailly, S.; Draghi, M.; Pestka, J.J.; Oswald, I.P.; Robine, E.; Bailly, J.D.; Lacroix, M.Z. Production of four macrocyclic trichothecenes by *Stachybotrys chartarum* during its development on different building materials as measured by UPLC-MS/MS. *Build. Environ.* **2016**, *106*, 265–273. [[CrossRef](#)]
39. Kumar, V.; Rao, P.K.; Rawal, A. Amplification of electrolyte uptake in the absorptive glass mat (AGM) separator for valve regulated lead acid (VRLA) batteries. *J. Power Sources* **2017**, *341*, 19–26. [[CrossRef](#)]
40. Zhu, J.; Yanilmaz, M.; Fu, K.; Chen, C.; Lu, Y.; Ge, Y.; Kim, D.; Zhang, X. Understanding glass fiber membrane used as a novel separator for lithium–sulfur batteries. *J. Membr. Sci.* **2016**, *504*, 89–96. [[CrossRef](#)]
41. Schadeck, U.; Kyrgyzbaev, K.; Gerdes, T.; Willert-Porada, M.; Moos, R. Porous and non-porous micrometer-sized glass platelets as separators for lithium-ion batteries. *J. Membr. Sci.* **2018**, *550*, 518–525. [[CrossRef](#)]
42. Zhang, S.S. A review on the separators of liquid electrolyte Li-ion batteries. *J. Power Sources* **2007**, *164*, 351–364. [[CrossRef](#)]
43. Cho, E.; Mun, J.; Chae, O.B.; Kwon, O.M.; Kim, H.-T.; Ryu, J.H.; Kim, Y.G.; Oh, S.M. Corrosion/passivation of aluminum current collector in bis(fluorosulfonyl)imide-based ionic liquid for lithium-ion batteries. *Electrochem. Commun.* **2012**, *22*, 1–3. [[CrossRef](#)]
44. Zhang, S.S. A review on electrolyte additives for lithium-ion batteries. *J. Power Sources* **2006**, *162*, 1379–1394. [[CrossRef](#)]
45. Kyrgyzbaev, K.; Rosin, A.; Willert-Porada, M. Influence of temperature on the thickness of ultrathin particulate glass platelets. *Glass Technol. Eur. J. Glass Sci. Technol. Part A* **2016**, *57*, 95–100. [[CrossRef](#)]



© 2018 by the authors. Licensee MDPI, Basel, Switzerland. This article is an open access article distributed under the terms and conditions of the Creative Commons Attribution (CC BY) license (<http://creativecommons.org/licenses/by/4.0/>).